Mon. Not. R. astr. Soc. (1988) **230,** 249–272

Spectral energy distributions of galaxies in high-redshift clusters – III. Abell 370 at z=0.37

Iain MacLaren and Richard S. Ellis *Department of Physics, University of Durham, South Road, Durham DH1 3LE*

Warrick J. Couch *Anglo–Australian Observatory, PO Box 296, Epping, NSW 2121 Australia*

Accepted 1987 August 31. Received 1987 July 28

Summary. We have imaged the distant cluster Abell 370 (z=0.37) with a CCD-based intermediate pass-band multicolour system defined in earlier papers in this series. Our technique is to use such colours to classify faint galaxies in redshift and spectral class without recourse to spectroscopic data. We demonstrate from a new comparison of ~80 spectra gathered in five clusters at high redshift (including Abell 370), that our photometric classifications are generally accurate to ±0.05 in redshift and to ±1 Hubble type. For Abell 370 we present classifications for a sample of over 100 galaxies, mostly cluster members, statistically complete to R_F=21.2. In addition we analyse a deep ultraviolet CCD image of the cluster; this image probes to ~250 nm in the cluster restframe. We find a significant fraction of the optically red galaxies, expected to be E/S0s from their position on the colour–luminosity sequence, show a flux enhancement of 0.5–2 magnitudes at 250 nm, an effect similar to that found in the cluster 0016+16 discussed in Paper II. We also confirm a significant excess of blue probable members with spectral characteristics similar to Scd spirals.

The coexistence in a single cluster of the high blue fraction, the red galaxies with ultraviolet excess *and* galaxies with intermediate colours and Balmer absorption features found by spectroscopic studies, suggests a single evolutionary track whereby galaxies undergo a burst of star formation decaying via the post-starburst and ultraviolet phase to normal E/S0s. The frequency of such behaviour supports the contention that we are witnessing the formation of S0s rather than an erratic evolutionary behaviour associated with normal ellipticals. However, the marked difference between the populations in 0016+16 and Abell 370 suggests such galaxy evolution occurs on locally determined time-scales.

1 Introduction

In the first paper in this series (Couch *et al.* 1983, Paper I) we developed a technique for constructing low-resolution spectral energy distributions (SEDs) of galaxies in distant clusters.

This was achieved by imaging the clusters in a set of intermediate bandwidth filters covering a large wavelength baseline (400–900 nm). Such an approach provides a spectral resolution intermediate to conventional broad-band photometry and low-resolution spectrophotometry. The wide wavelength coverage allows selection of objects of various redshifts/spectral classes for further study and enables monitoring of the global evolution of populations of objects. This provides a considerable advance over much previous work which has tended to concentrate on the evolutionary status of only the brightest cluster galaxies. These usually lie in the central regions of rich clusters and may suffer from dynamical processes that render them atypical for evolutionary work. With our technique we image typically 75–100 galaxies per exposure. By probing further down the cluster luminosity function in this manner we obtain information relevant to the evolution of more normal cluster galaxies.

Applying this SED technique to the distant $z=0.54$ cluster 0016+16 (Ellis *et al.* 1985, Paper II) we were able to assign an appropriate redshift and 'spectral class' (in the sequence E/S0, Sab, Sbc, Scd, Sdm) to each object to an accuracy sufficient to distinguish probable cluster members from contaminating field objects. Indeed we discovered the presence of a substantial amount of foreground contamination at $z\sim0.2$–0.3 in the field of 0016+16 which was previously unsuspected and now supported by further redshift work in the field around 0016+16. Furthermore, we could clearly distinguish the colour–magnitude (CM) sequence in a range of colours allowing not only very good selection criteria for E/S0 cluster members but also enabling us to investigate the wavelength dependence of the CM-effect. In this respect our results were somewhat surprising. Specifically we found that many of the early-type cluster members were substantially brighter in the rest frame ultraviolet ($\lambda_{\rm rest}\sim270$ nm) than suggested by ultraviolet observations of nearby E/S0s. Such finding is of great significance for evolutionary studies since, as we suggested in Paper II, it may be interpreted as evidence for higher rates of star formation in the past.

In this paper we shall be concerned with the cluster Abell (A)370, which at $z=0.37$, is one of the most distant in Abell's catalogue. It has a striking appearance (Plate 1a) – rich and dominated by two central luminous members. At such a redshift we are able to view the properties of many early-type galaxies some 5 Gyr ago (here and in what follows $H_0=50$, $q_0=0.1$). Single-colour broad-band photographic photometry has already been carried out in A370 by Couch (1981), Couch & Newell (1984, hereafter CN) and Butcher & Oemler (1984). These studies revealed that the cluster exhibits a substantially large fraction of blue objects ($f_b\sim0.2$, in Butcher & Oemler's notation), more than expected on the basis of nearby clusters of similar structure (see Couch 1981 for details).

The interpretation of blue fractions based on a single-colour distribution as a manifestation of imprecise field subtraction rather than an intrinsic property of such clusters was first discussed by Mathieu & Spinrad (1980). Subsequently multiple object spectroscopy has been used to resolve the field contamination question (Dressler & Gunn 1982, 1983; Dressler *et al.* 1985; Sharples *et al.* 1985) particularly in the original two Butcher–Oemler (B–O) clusters Cl 0024+16 and 3C 295. Some spectroscopy is also available for A370 (see Section 5 for discussion). Each of these studies generally upholds the B–O effect but by varying amounts of statistical significance. Spectroscopy is a powerful tool in this programme but typically only 20–30 galaxies are accessible in each cluster to the spectroscopic limit of a 4-metre telescope so it is best used in conjunction with deeper photometric studies.

A370 is an ideal candidate for our multicolour photometry, contrasting the properties of 0016+16, which is redder and has no substantial blue fraction. Bautz, Loh & Wilkinson (1982) have also obtained multicolour CCD photometry of this cluster, but only for the brightest ~20 galaxies in the cluster field. They also, tentatively, claim to uphold the Butcher–Oemler effect. A further motivation for studying it is to check whether the ultraviolet (UV) scatter observed in the

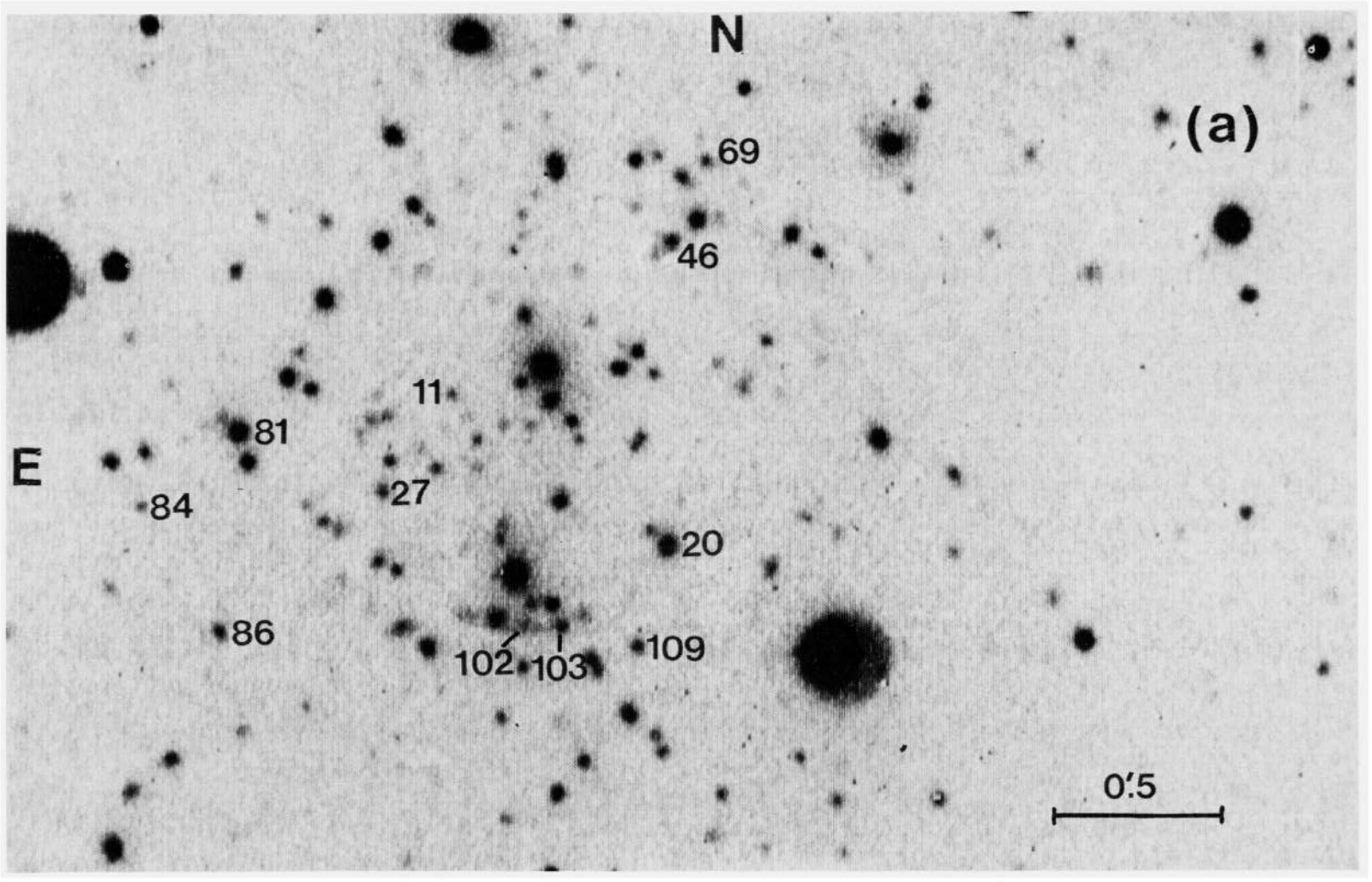

Plate 1. CCD images of Abell 370 taken with the AAT: (a) in the 685 nm filter with UVX E/S0s to R_F=21.2 marked; (b) in broad band U.

[facing page 250]

1988MNRAS.230..249M

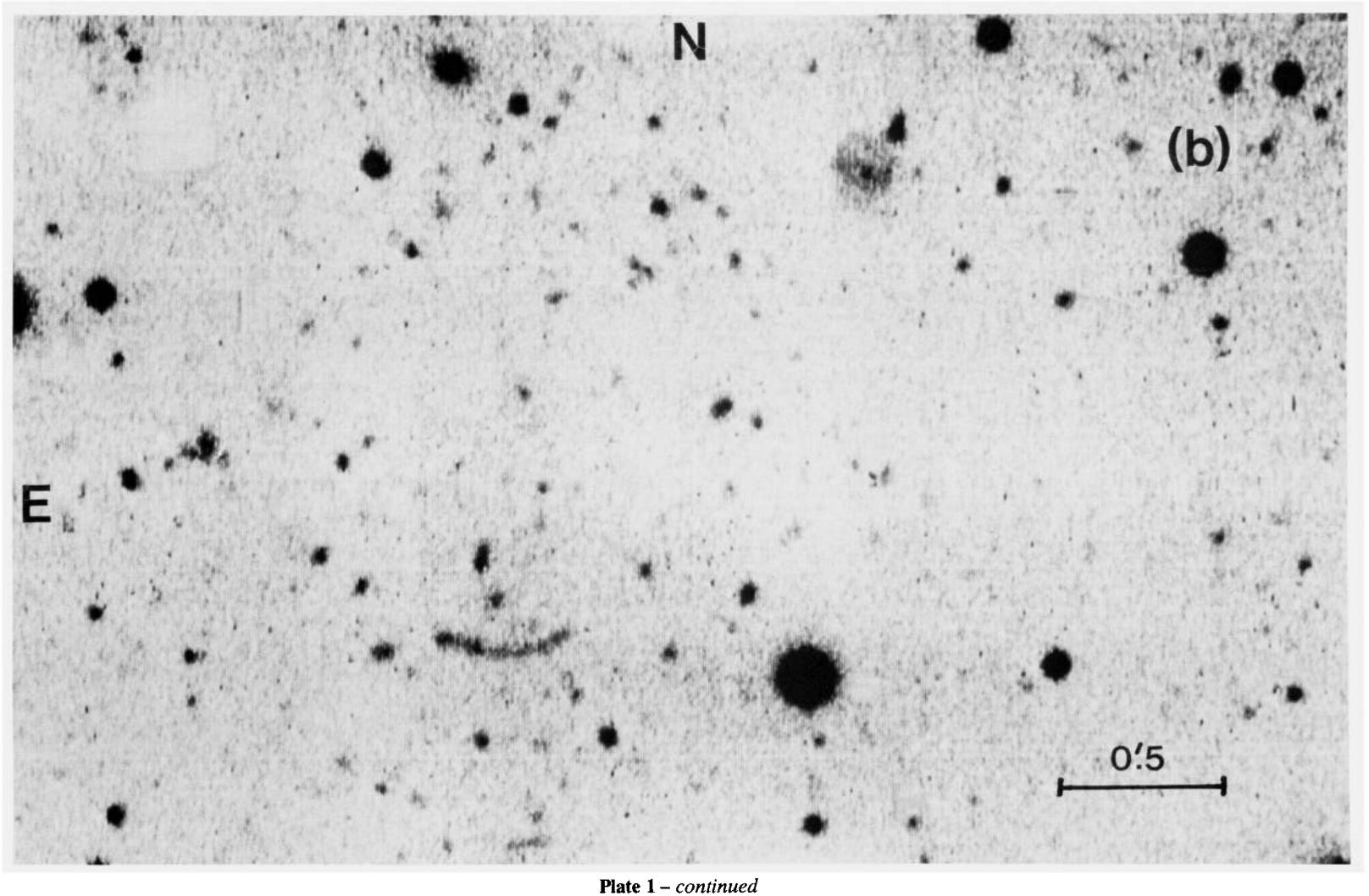

Plate 1 – *continued*

0016+16 E/S0s is a general property of early-type galaxies at high redshift. A370 is a rich cluster at a redshift just sufficient for ground-based studies to probe the same rest frame UV wavelength (260 nm) studied in 0016+16 but with an improved signal-to-noise ratio (S/N). It is interesting to note that, via such techniques, we are amassing UV photometric information on larger samples of galaxies than those available nearby using the *IUE* satellite. Detailed UV studies of clusters at redshifts $z<0.3$ must await the launch of the *Space Telescope*.

In this paper we present a study of a complete sample of about 100 galaxies in the field of A370. In the next section we outline the observational details, precision and completeness of our photometry. In Section 3 we discuss the SED classifications, foreground reddening and the present-day UV colour–magnitude relation. In Section 4 we construct the cluster colour–magnitude diagrams, and compare with the available spectroscopy in Section 5 before discussing the implications for galaxy evolution in Section 6.

2 Observations and data reduction

2.1 LOG OF OBSERVATIONS

As in previous papers, our photometry is based on a system using the RCA CCD at the prime focus of the 3.9-m Anglo–Australian Telescope and a set of intermediate bandwidth filters described in Papers I and II. Here we imaged A370 in four of these filters at 418, 502, 685 and 862 nm. From simulations, we found that photometry in these four pass-bands is sufficient to adequately resolve contaminating field galaxies from probable cluster members at $z\sim0.4$. Since A370 is at lower redshift than 0016+16, our previously bluest band (418 nm) does not penetrate sufficiently far into the rest frame ultraviolet to test for the presence of UV enhancements of the kind found in 0016+16. Consequently we have also imaged the cluster in the Johnson *U*-band which reaches rest wavelengths (~260 nm) similar to those attained in 0016+16. This filter is somewhat broader than our intermediate bands. However, we shall not use the *U* photometry as part of our object classification scheme, but rather as an indicator of the UV flux from galaxies selected and classified using the other four intermediate pass-bands.

Table 1 summarizes our observations, made during two runs in 1983 October and 1985 December. Repeated observations of Oke (1974) spectrophotometric standard stars (VMa 2 and

Table 1. Log of observations.

Object	Date	Filter	Exposure(s)	Airmass	Seeing (arcsec)
A370	1983 October 8/9	502	1400	1.22	1.02
		685	1200	1.27	1.52
		862	1200	1.33	1.14
VMa2	1983 October 8/9	502	10 (×6)	1.25–1.82	0.79
		685	10 (×4)	1.25–1.79	0.83
		862	20 (×3)	1.25–1.84	0.81
A370	1985 December 13/14	*U*	1000 (×2)	1.15–1.17	1.57
		U	2000	1.15	1.60
		418	1000	1.20	1.6
		685	800	1.26	1.66
VMa2	1985 December 13/14	*U*	25 (×2)	1.32	1.8
		418	50 (×2)	1.34	1.98
		685	30 (×2)	1.34	1.70
Feige 24	1985 December 13/14	*U*	25 (×2)	1.22	1.86
		418	30 (×2)	1.22–1.43	1.80
		685	30 (×4)	1.22–1.42	1.80

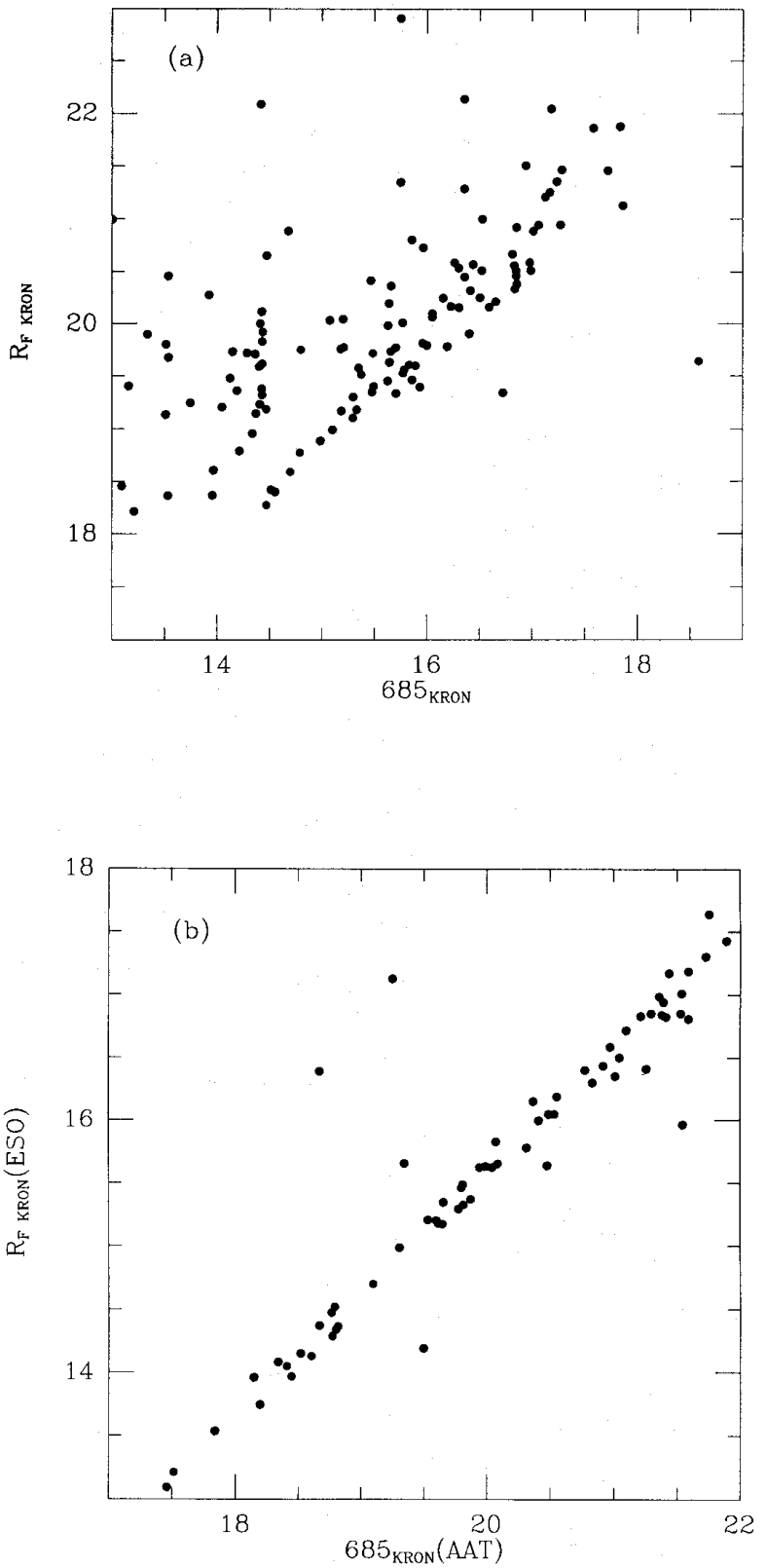

Figure 1. Photometric calibration of the CCD data. (a) Couch & Newell's photographic R_F photometry compared with that in the CCD 685 nm system; both magnitudes are Kron-style. The large scatter arises from crowding difficulties (see text). (b) ESO 3.6-m *R* CCD magnitudes compared with AAT 685 nm magnitudes justifying the high precision of the CCD photometry. (c) 4.8 arcsec diameter aperture magnitudes in the AAT 685 nm system compared with Couch and Newell's photographic Kron magnitudes. The solid line represents the adopted calibration between the two scales.

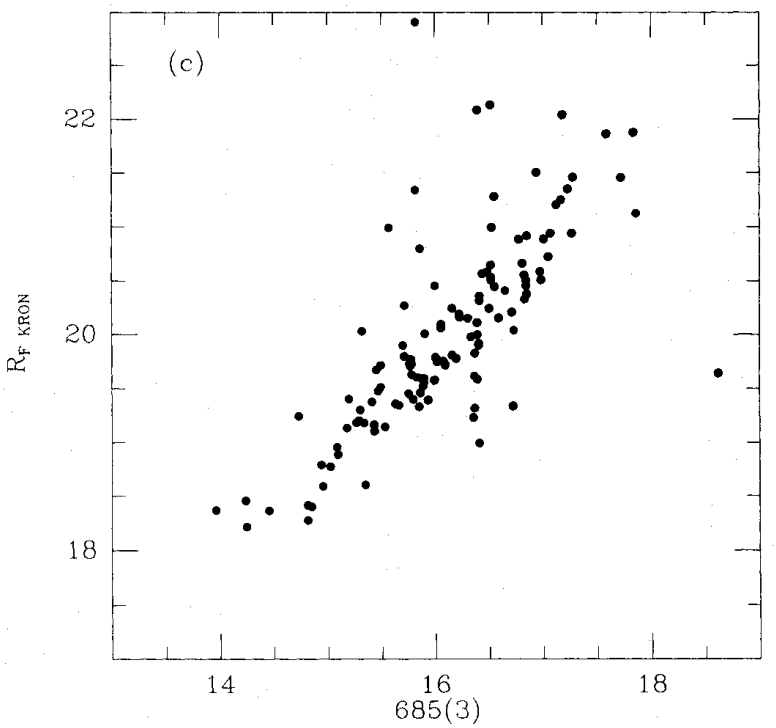

Figure 1–*continued*

Feige 24) throughout each night provided zero points for our photometry as well as a monitor of the stability of the photometric conditions.

2.2 REDUCTION PROCEDURE

Our data reduction procedures are discussed in detail in Papers I and II. We briefly outline them here for completeness. The observations of A370 and the standard stars were reduced using the STARLINK ASPIC image processing routines and the APEX-based photometry package of Newell (1979) and CN.

After removal of cosmic ray events and correction for CCD cosmetic defects, the frames were individually flat-fielded and interference fringes removed from the 685 and 862 frames by subtracting a suitably scaled zero-meaned exposure of a blank sky field in each filter.

The 685 nm CCD image is shown in Plate 1(a). This frame was used to select objects for study, the APEX software providing 10 aperture magnitudes and a Kron (1978) style total magnitude for each chosen galaxy. Note that the cluster core is off-centre on the frame in order to avoid the two central defective columns present on this CCD. Unfortunately there is also a small positional offset between the two observing runs which means that some of the objects are not present in all pass-bands. In what follows, however, we will consider only those objects in the 3.75×2.00 arcmin area common to both runs.

The similarity of our 685 filter to CNs R_F band allows us to calibrate our 685 mag against their photographic photometry. A comparison of the Kron magnitudes derived from both sets of photometry would be most appropriate but suffers from the complication of image-crowding. Contamination of objects by close neighbours is a severe problem in A370 and in order to deal with it (as in all their clusters) CN applied a cleaning algorithm to their data before magnitude measurement. We are not able to apply this algorithm in our reductions as it is not suited to CCD-type data (Newell 1982). As a consequence the Kron magnitudes for many of our objects are

systematically too bright due to neighbours falling within the Kron radius. This effect can be seen in Fig. 1(a) where we plot CN's R_F Kron magnitudes against the equivalent 685 values measured here. The contaminated objects form a clear group which scatter upwards from a ridge line of objects which define a one-to-one relationship between the two scales. Visual inspection of these objects confirms that crowding is responsible.

A further check on the integrity of the CCD data is provided by a R-band CCD exposure taken by Couch, Ellis & D'Odorico (1987, unpublished) on the ESO 3.6-m telescope at La Silla. Whilst standards taken on that occasion reveal conditions to be non-photometric, we can verify the quality of the AAT CCD photometry on a relative scale by plotting R(ESO) versus R_F(AAT) – Fig. 1(b). The good agreement confirms the discrepancy in Fig. 1(a) is not a consequence of poor quality CCD data.

In order to obtain a zero point unaffected by crowding it is necessary to consider magnitudes measured within an aperture small enough, in general, to exclude neighbouring images. In Fig. 1(c) we plot the 685 magnitudes measured in the third smallest (4.8 arcsec) aperture against CN's R_F Kron magnitudes and we see a much tighter relation. Indeed we regard it to be sufficiently tight to adopt the mean one-to-one relation fitted to the data as the calibration between our 685 magnitudes and the R_F Kron scale:

$$685(3)=R_F(\text{Kron})-3.93\pm0.05. \quad (1)$$

Fortunately a check on this calibration is available to us as a result of an R magnitude – on the Kron–Cousins system – for our spectrophotometric standard star VMa2, $R_{KC}=12.129\pm0.005$, kindly obtained for us by H. Morrison (1986, private communication). After accounting for the colour equation between R_{KC} and CN's R_F band (Couch & Newell 1980), we find

$$685(\text{Kron})=R_F(\text{Kron})-4.04\pm0.007. \quad (2)$$

The two relations (1) and (2) thus appear to be consistent; we can therefore safely estimate total magnitudes from our 685(3) measures.

Finally, we can use the comparison with Couch to assess the completeness limits of both sets of data. Couch claimed his photographic photometry is complete to $R_F=21.2$. We find 105 objects in our CCD area to this limit, including seven objects undetected by Couch. Only one object (No. 43) found in the photographic data has no CCD counterpart. Thus assuming the CCD data are complete to at least $R_F=21.2$, we can first conclude Couch is 6 per cent incomplete at this limit.

The completeness of the CCD data beyond $R_F=21.2$ can be assessed in two ways. First we can assess the number magnitude counts within the cluster and compare with those in 0016+16 (Paper II, fig. 6) where the completeness limit is known to be $F=22.5$ ($R_F=22.1$). Table 2 shows the measured counts in the CCD area and the expected level of field contamination (based on field count data – CN). The cluster luminosity functions can be compared making allowance for the

Table 2. Integral number of counts in CCD field.

R_F	Number measured	Expected field
20.0	50	5
20.5	75	8
21.0	97	13
(21.2	102	18)
21.5	110	19
22.0	130	–

Note: Photographic incompleteness beyond $R_F=21.5$ makes it difficult to predict fainter field counts.

difference in distance modulus. Ignoring any evolution between the two, there is slight evidence for a flatter slope in the A370 data beyond R_F=21.5–22.0. This limit also agrees with that derived from the 685 exposure times used for A370 and 0016+16 (1200 and 2000 s respectively) which indicates a completeness limit of R_F=21.7 to the same S/N. In this paper, therefore, we will adopt R_F=21.7 as a reasonable estimate of the completeness limit of our CCD photometry. As in Paper II, however, we restrict the SED analysis to a sample limited 0.5 mag brighter than the completeness limit, namely R_F=21.2. This yields 102 objects for detailed examination.

2.3 ERRORS

In our previous work we have conducted detailed comparisons of repeat exposures in our various pass-bands to determine photometric random errors. We concluded that the errors are not significantly larger than those expected from photon-noise considerations (see Papers I and II). Errors in the intermediate-band filters determined for 0016+16 were found to be ~0.07 mag (0.12 mag in 418) down to a limit slightly deeper than that attained here in A370 (note that the 1983 observations of A370 were obtained on the same night as many of the 0016+16 exposures of Paper II).

For our investigations of the form of SEDs at high redshift, the *U* pass-band is of most importance. Thus it is crucial to ensure accurate error determinations for this filter. We obtained three individual exposures (one at 2000 s and two at 1000 s) for this purpose. At R_F=21.2 we find the scatter in *U* (scaled to the total exposure of 4000 s) is ~0.21 mag, whereas the expected Poisson value is ~0.20. Note, however, that the errors in *U* are not a straightforward function of R_F since these bands are well separated in wavelength. Thus for a fixed R_F an object with bluer colours has a better-defined *U* magnitude than a redder object. Here, we simply note that the photometric uncertainty for any colour can be adequately estimated from photon-noise consideration. We will return to this point in Section 4 when we discuss the UV–optical colour luminosity relation.

The photometric quality of the data can be assessed by noting that the repeat exposures of the spectrophotometric standards taken on both runs yield results in good agreement. Again this is most critical at short wavelengths where the extinction is largest. In *U*, 418 and 685, the two standards VMa2 and Feige 2 give colour offsets consistent to between 0.01 and 0.04 mag.

3 Results

3.1 SEDS AND OBJECT CLASSIFICATION

We use the magnitudes determined in our pass-bands to construct low resolution SEDs for all the galaxies in our sample. Our observations can be compared directly with colour predictions obtained on the basis of appropriate *k*-corrected spectra of nearby galaxies of various morphological types (Pence 1979; Coleman *et al.* 1980). The necessary zero points are determined from our standard stars.

Our technique is to plot the observed colours and the *k*-corrected spectra for a wide range of redshift (see fig. 5 of Paper II). This enables us to assign a most probable redshift and spectral class to each galaxy from the best fit to the SED. Whilst we include the *U* colour for each galaxy on our SED plots (Fig. 2) we stress that *our classification is based on the use of intermediate bandwidth filters only*, i.e. excluding the *U* magnitudes. The classifications obtained in this manner are accurate to approximately ±0.05 in *z* and to within a single Hubble class (see Paper II), which is sufficient in most cases to determine whether a given object is a cluster member, and if so, of what type. The A370 classifications are summarized in Table 3 and a representative sample of SEDs is shown in Fig. 2.

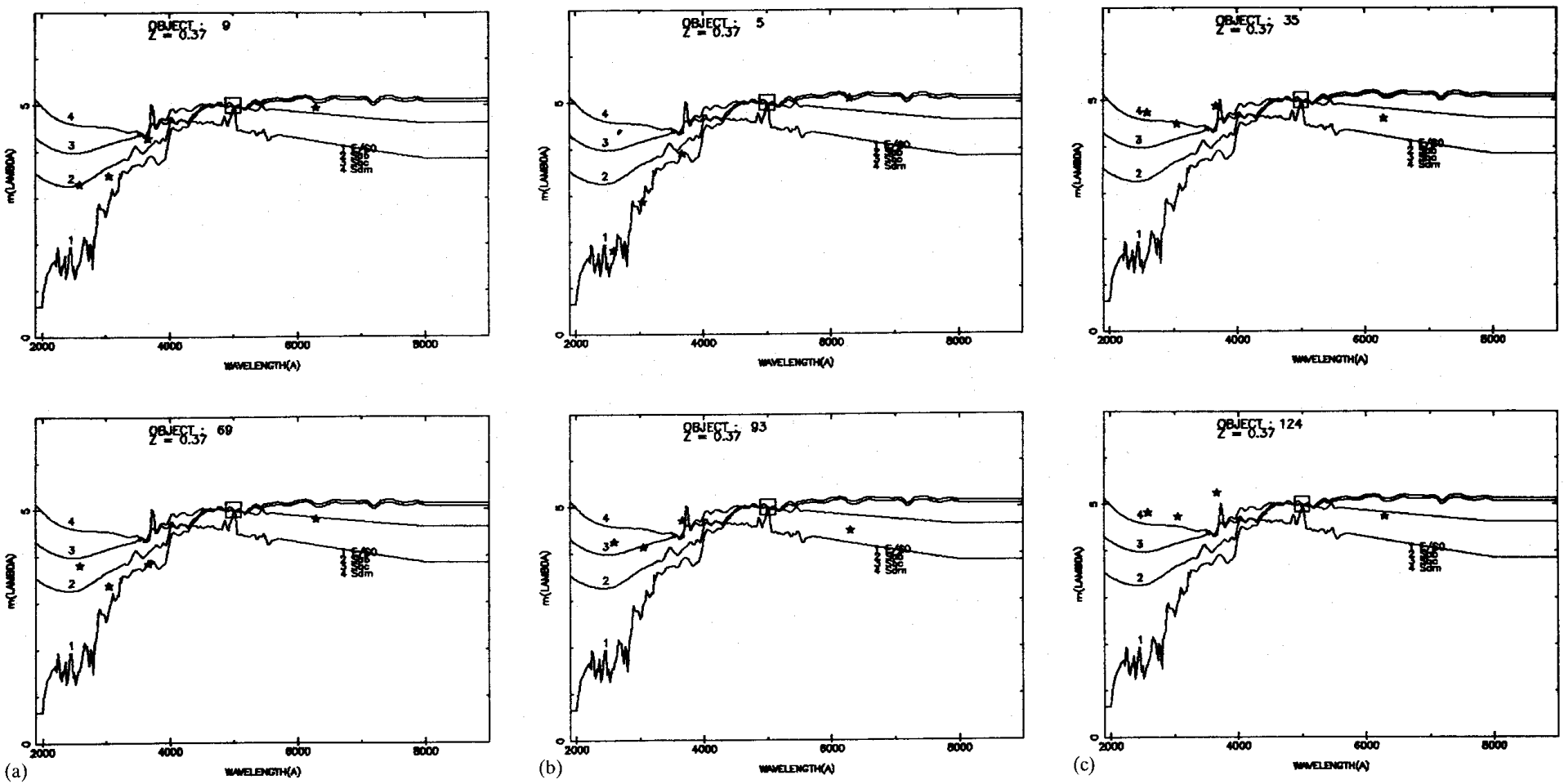

Figure 2. A representative sample of spectral energy distributions for galaxies in Abell 370; the R_F magnitude, adopted redshift and class are marked in each example. The curves represent the SEDs of present-day galaxies of various morphologies (see legend) and all data is presented in the rest frame and standardized at the corresponding rest wavelength of the 685 nm band.

Table 3. A370 galaxy classifications.

CCD#	BO#	RA(1950)			Dec(1950)			R_F	z	Type
128	16	02	37	13.9	-01	48	2.8	17.845	0.00	Star
107	9	02	37	20.6	-01	47	48.1	18.453	~0.37	E/S0
1	10	02	37	20.2	-01	47	10.6	18.470	~0.37	E/S0
53	15	02	37	15.9	-01	46	32.1	18.621	~0.25	E/S0
81	–	02	37	24.0	-01	47	18.5	18.820	~0.37	E/S0+uv
125	21	02	37	16.2	-01	47	25.5	18.880	~0.37	E/S0
20	29	02	37	18.8	-01	47	43.5	18.901	~0.37	E/S0+uv
47	34	02	37	18.3	-01	46	45.0	18.992	~0.37	E/S0
42	24	02	37	20.0	-01	46	33.9	19.028	~0.37	E/S0
31	26	02	37	22.8	-01	46	57.2	19.044	~0.37	E/S0
32	43	02	37	22.1	-01	46	47.1	19.124	~0.37	E/S0
66	39	02	37	21.9	-01	46	27.8	19.166	0.2-0.4	Scd
29	41	02	37	23.3	-01	47	11.1	19.193	~0.37	E/S0
49	45	02	37	17.2	-01	46	48.1	19.265	~0.37	E/S0
137	56	02	37	11.7	-01	47	1.5	19.294	~0.37	Sab
94	–	02	37	21.7	-01	48	0.6	19.306	~0.37	E/S0
15	61	02	37	19.3	-01	47	11.6	19.331	~0.37	E/S0
3	–	02	37	20.2	-01	47	16.5	19.341	~0.37	E/S0
55	37	02	37	17.7	-01	46	21.5	19.358	~0.37	E/S0
80	–	02	37	23.9	-01	47	20.7	19.376	~0.37	E/S0
102	49	02	37	20.8	-01	47	55.8	19.377	~0.37	E/S0+uv
36	245	02	37	21.5	-01	46	43.6	19.396	~0.37	E/S0
68	66	02	37	19.0	-01	46	33.5	19.407	~0.37	E/S0
22	63	02	37	20.0	-01	47	34.9	19.442	~0.37	E/S0
83	70	02	37	25.3	-01	47	26.2	19.455	~0.37	E/S0
54	–	02	37	15.6	-01	46	24.1	19.486	~0.37	Scd
105	–	02	37	20.2	-01	47	53.3	19.535	~0.37	E/S0
14	84	02	37	19.1	-01	47	8.5	19.571	~0.25	E/S0
12	80	02	37	20.4	-01	47	1.0	19.628	~0.37	E/S0
46	256	02	37	18.6	-01	46	48.5	19.668	~0.37	E/S0+uv
27	544	02	37	22.1	-01	47	32.3	19.730	~0.37	E/S0+uv
86	106	02	37	24.2	-01	47	56.8	19.739	~0.37	E/S0+uv
28	111	02	37	23.0	-01	47	13.5	19.785	~0.37	E/S0
144	–	02	37	12.7	-01	46	29.0	19.796	0.3-0.4	Sab
4	58	02	37	19.9	-01	47	20.7	19.801	~0.37	E/S0
50	99	02	37	16.9	-01	46	51.1	19.827	~0.37	E/S0
70	128	02	37	18.4	-01	46	37.0	19.833	~0.37	Scd
110	94	02	37	19.7	-01	48	4.1	19.834	~0.37	E/S0
82	115	02	37	25.0	-01	47	23.8	19.838	0.2-0.4	Scd/Sdm
133	113	02	37	11.8	-01	47	41.0	19.854	~0.37	Sab
2	–	02	37	20.5	-01	47	13.7	19.880	~0.37	E/S0
127	148	02	37	10.9	-01	48	9.5	19.903	~0.37	E/S0
126	102	02	37	15.3	-01	47	32.0	19.915	~0.37	E/S0
106	–	02	37	20.4	-01	47	53.4	19.926	~0.37	E/S0
6	124	02	37	19.1	-01	47	24.4	19.945	0.3-0.4	E/S0
108	176	02	37	20.7	-01	47	41.3	19.964	~0.37	Scd
124	151	02	37	17.5	-01	47	48.2	19.966	0.2-0.4	Scd/Sdm
93	128	02	37	22.0	-01	47	56.7	19.978	~0.37	Scd
91	119	02	37	22.0	-01	47	46.6	19.982	~0.37	E/S0
26	–	02	37	22.0	-01	47	27.1	19.986	~0.37	E/S0
18	166	02	37	17.5	-01	47	7.3	20.028	~0.37	E/S0
90	165	02	37	22.2	-01	47	44.9	20.033	~0.37	Scd
79	149	02	37	23.8	-01	46	51.5	20.043	~0.37	E/S0
138	145	02	37	13.6	-01	46	56.5	20.047	~0.37	Sbc
69	131	02	37	18.1	-01	46	34.2	20.049	~0.37	E/S0+uv
109	142	02	37	19.2	-01	48	1.5	20.100	~0.37	E/S0+uv
16	–	02	37	18.9	-01	47	12.9	20.154	~0.37	E/S0
88	161	02	37	22.9	-01	47	37.7	20.161	~0.37	E/S0
33	153	02	37	22.7	-01	46	42.9	20.187	~0.37	E/S0
23	133	02	37	21.5	-01	47	28.1	20.195	~0.37	E/S0
21	154	02	37	19.0	-01	47	40.9	20.243	~0.37	E/S0
103	–	02	37	20.5	-01	47	56.7	20.302	~0.37	E/S0+uv
19	164	02	37	17.8	-01	47	15.0	20.330	~0.37	Sbc/Scd
9	232	02	37	21.0	-01	47	23.4	20.332	~0.37	Sab
252	–	02	37	6.9	-01	47	46.6	20.334	~0.37	E/S0
84	203	02	37	25.0	-01	47	33.8	20.376	~0.37	E/S0+uv
35	55	02	37	21.7	-01	46	41.1	20.399	~0.37	Scd

Table 3–*continued*

CCD#	BO#	RA(1950)			Dec(1950)			R_F	z	Type
89	226	02	37	22.7	-01	47	39.0	20.401	~0.37	Scd
30	213	02	37	23.1	-01	47	6.7	20.416	~0.3	E/S0
250	–	02	37	4.9	-01	48	5.0	20.433	0.2-0.4	Scd
71	168	02	37	18.8	-01	46	32.8	20.445	~0.37	E/S0
140	201	02	37	14.3	-01	46	34.9	20.473	~0.37	Scd/Sdm
24	247	02	37	22.1	-01	47	18.8	20.475	0.2-0.4	Scd?
11	219	02	37	21.3	-01	47	15.5	20.496	~0.37	E/S0+uv
52	–	02	37	15.8	-01	46	40.4	20.499	~0.37	E/S0
292	314	02	37	20.9	-01	50	5.7	20.511	>0.5	Scd
85	239	02	37	25.4	-01	47	48.1	20.529	~0.37	Scd
275	329	02	37	17.2	-01	49	41.9	20.573	0.2-0.4	Scd
25	–	02	37	22.4	-01	47	21.6	20.583	~0.37	Scd
274	–	02	37	9.5	-01	46	54.8	20.599	0.2-0.4	Scd/Sdm
245	235	02	37	9.4	-01	48	8.0	20.604	>0.5	Sab
5	230	02	37	19.8	-01	47	23.4	20.609	~0.37	E/S0
77	–	02	37	24.8	-01	46	56.4	20.663	0.2-0.4	Scd
101	–	02	37	21.2	-01	47	54.9	20.664	0.2-0.4	Scd
10	238	02	37	21.0	-01	47	28.5	20.702	~0.37	E/S0
100	136	02	37	20.5	-01	48	4.6	20.712	~0.37	Scd
139	231	02	37	14.8	-01	46	49.2	20.736	~0.37	Scd
13	255	02	37	19.7	-01	47	2.5	20.782	~0.37	E/S0
57	293	02	37	20.1	-01	46	17.3	20.796		Steep spectrum
17	308	02	37	18.1	-01	47	10.9	20.801	~0.37	E/S0
45	256	02	37	18.8	-01	46	50.7	20.802	0.2-0.4	Scd
87	311	02	37	23.1	-01	47	34.5	20.840	~0.37	E/S0
40	220	02	37	20.4	-01	46	43.3	20.865	~0.37	E/S0 (no U)
8	363	02	37	20.7	-01	47	20.9	20.872	~0.3	E/S0
78	257	02	37	23.5	-01	46	42.0	20.882	~0.37	E/S0-Sab
123	249	02	37	17.1	-01	47	39.1	20.884	~0.37	Sab
56	280	02	37	19.6	-01	46	16.3	20.927	0.5-0.6	Sbc
37	–	02	37	21.6	-01	46	52.1	21.092	~0.5:	E/S0:
122	316	02	37	16.7	-01	47	41.9	21.108	~0.37	E/S0
41	251	02	37	20.2	-01	46	39.8	21.113	~0.37	E/S0
44	372	02	37	19.7	-01	46	53.3	21.139	0.2-0.4	Scd
51	409	02	37	16.3	-01	46	52.5	21.197	~0.6	Sbc
39	227	02	37	20.5	-01	46	49.3	21.203	~0.37	E/S0
249	–	02	37	6.5	-01	48	0.3	21.215	~0.37	Sdm
132	–	02	37	12.7	-01	47	44.3	21.299	~0.37	Sab
257	53	02	37	9.4	-01	47	5.2	21.332	~0.37	E/S0
261	–	02	37	7.0	-01	46	47.7	21.344	~0.37	Scd/Sdm
67	303	02	37	19.1	-01	46	41.7	21.385	0.5-0.6	E/S0
246	126	02	37	10.1	-01	48	1.4	21.473	~0.37	E/S0
251	183	02	37	5.7	-01	47	42.7	21.478	~0.37	E/S0
290	427	02	37	22.6	-01	50	17.6	21.506	>0.5	Scd/Sdm
258	78	02	37	8.5	-01	47	7.2	21.582	>0.45	E/S0
141	–	02	37	14.5	-01	46	29.9	21.619	0.75?	Sab
263	–	02	37	5.0	-01	47	1.8	21.664	~0.37	Sbc/Scd
280	262	02	37	17.8	-01	49	55.4	21.697	0.4-0.6	Sbc
284	208	02	37	24.3	-01	49	41.2	21.782	~0.37	Scd
297	187	02	37	19.0	-01	50	39.5	21.822	~0.37	Scd
295	–	02	37	18.2	-01	50	30.5	21.879	~0.37	Scd
282	425	02	37	18.8	-01	49	40.3	21.943		Steep Spectrum
287	40	02	37	24.7	-01	50	4.9	22.184	~0.37	E/S0
281	–	02	37	19.0	-01	49	43.1	22.211	~0.37	Scd/Sdm

The precision and accuracy of such classifications as assessed by independent spectroscopy was briefly addressed in Paper II, where unpublished data from Dressler & Gunn on the cluster 0016+16 was discussed. Since that work, we have accumulated a catalogue of spectra for objects classified via the SED technique and we will discuss these, along with spectroscopy for galaxies in A370, in Section 5.

3.2 THE COLOUR–MAGNITUDE EFFECT

In our previous work we have used the well known colour–magnitude (CM) relation for early-type galaxies (Visvanathan & Sandage 1977) as a diagnostic tool for galaxy evolution. In the case of 0016+16 the CM effect at optical wavelengths enabled us to select a clearly defined sequence of early-type galaxies for study in the rest frame UV. We will now undertake a similar analysis for the present data.

For comparison of the observed CM-relation with that expected from studies of nearby early-type galaxies we have to consider two important factors: (a) the amount of foreground reddening present, and (b) the nature of the CM relation in the ultraviolet.

(a) Foreground reddening

Estimates of the foreground reddening to A370 are available to us through (i) the work of Couch (1981) who, from a study of the colour distribution of field galaxies in the vicinity of A370, derived a reddening of $E(B-V)=0.12\pm0.05$, and (ii) the method we have developed in Papers I and II for measuring the reddening directly from the observed SEDs using colours redward of ~685 nm.

In the latter case we follow the procedure of Paper II where we combine optical and infrared photometry through similar apertures to provide a long wavelength baseline. Couch & Sharples (1987, unpublished) have observed 11 of the galaxies in our sample at H (and in some cases J and K) using a 4.5 arcsec aperture. Ten of these are classified as E/S0s in Table 3. Using Seaton's (1981) reddening law we calculate a mean $E(B-V)$ for each object using a redshifted present-day E/S0 SED as a reference. The precision of the value of $E(B-V)$ so derived is ~10 per cent for an individual measurement.

We find this method gives results which are reasonably consistent, both from object to object and with infrared wavelength within a given object. However, surprisingly, the reddening inferred is negative with a mean value $\langle E(B-V)\rangle=-0.014\pm0.020$. Clearly there is some systematic discrepancy in the optical-infrared comparison. Since our data are standardized at 685 nm, a zero-point offset of 0.16 mag (in the sense of our 685 magnitudes being too bright) would reconcile this negative result with Couch's value above. However, later we will find very good agreement between the optical CM relations and those predicted from the same SEDs. Unless the entire optical or infrared scales are systematically in error, the cause must lie with the present-day SEDs used in the comparison. In the near infrared region these are poorly defined; a blueing of 0.16 mag in $R-H$ cannot be ruled out (*cf.* Lilly & Longair 1984). In the remainder of the discussion we shall adopt Couch's $E(B-V)$ value since our CM data provide some support for a correction of this size.

(b) The UV CM-relation

Visvanathan & Sandage's (1977) study of the CM relation for early-type galaxies is limited to the optical region ($\lambda>330$ nm), whereas we probe into the rest-frame UV of the A370 galaxies. As before, we use the method developed by Couch (1981) to determine the expected UV–optical relation. This is done by mixing the UV–optical spectra of M31 and the metal poor globular cluster M15 in linear proportions to mimic SEDs of galaxies at intermediate luminosities.

Using UV spectra gathered from the *IUE* archive, it is now possible to construct an observed UV CM relation. Table 4 shows our selection of normal E galaxies for which *IUE* long wavelength spectra (190–320 nm) of adequate S/N are available. Each spectral image has been reduced using the standard reduction procedure IUEDR available on the STARLINK network. Optical CCD photometry of these galaxies in an aperture similar to that used by *IUE* has been kindly supplied by D. Burstein (1986, private communication). To facilitate comparisons with the UV–optical

Table 4. Catalogue of *IUE* spectra for nearby E/S0s.

NGC	IUE Image	min	BT	AB	V(IUE)	UV(0.37)	Mv
1553	LWR15381	303	10.47	0.00	11.78	29.62	-22.17
4278	LWR11055	421	11.15	0.10	12.18	29.89	-20.32
4889	LWP1524	368	12.45	0.05	13.49	31.44	-24.06
4125	LWR13025	420	10.70	0.04	12.59	30.07	-22.62
4552	LWR13622	370	10.81	0.14	12.01	29.56	-17.64
205	LWR17019	270	8.65	0.14	13.49	29.77	-14.54
221	LWR3111	380	9.15	0.31	10.30	27.99	-14.13
4374	LWR4777	400	10.31	0.13	11.83	29.66	-21.72
224	LWR6343	340	4.36	0.31	10.28	28.51	-22.40
4472	LWR6877	360	9.31	0.00	11.62	29.46	-22.76
4472	LWR6912	330	9.31	0.00	11.62	29.35	-22.76
4621	LWP8129	350	10.75	0.07	12.10	29.18	-19.35
6166	LWR1372	792	13.05	0.00	14.65	30.69	-24.24
4382	LWR9381	300	10.10	0.04	11.84	29.30	-21.69

CM relation for A370, we passed the *IUE* spectra through a band-pass equivalent to the rest-frame response of our *U* filter at $z=0.37$.

The derived UV–optical CM-relation including corrections for reddening and redshift effects (Fig. 3) shows a slope in good agreement with Couch's predictions. The former scatter about the mean relation is 0.25 mag. It should be noted, however, that the intrinsic spread may well be somewhat less in cluster samples since we have not corrected for the range of metric aperture sizes covered in the *IUE* sample which is drawn from galaxies at a range in distance.

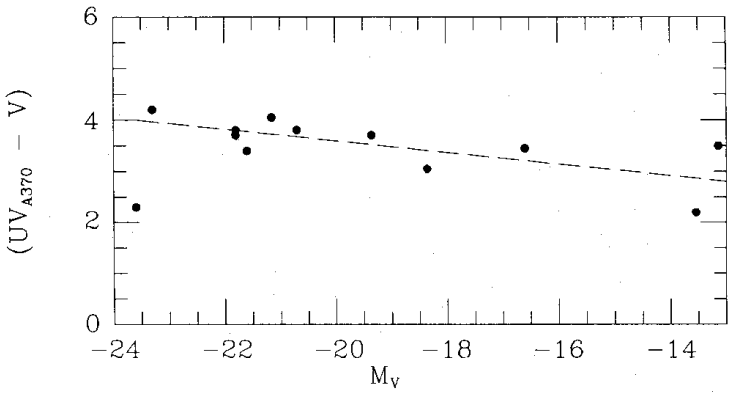

Figure 3. Ultraviolet–optical colour–luminosity relation for present-day early type galaxies derived from *IUE* spectra analysed by one of us (IM) and optical photometry corrected to the *IUE* aperture kindly supplied by David Burstein. Colours are corrected for effects of redshift and galactic extinction. The dashed line is the expected relation derived using Couch's synthesis method (see text).

4 Analysis

4.1 FOREGROUND CONTAMINATION AND THE BUTCHER–OEMLER EFFECT

In our sample of 102 galaxies to $R_F=21.2$ (Table 3) our SED procedure reveals 78 cluster members, a further 13 with uncertain membership (being classified $z\sim0.2=0.4$), 9 non-cluster members, 1 unclassified steep-spectrum object and 1 star. The total field galaxy component, therefore, lies somewhere between 10 and 24 objects depending on the status of the uncertain members. This is to be compared with the 18 predicted from CN's photographic photometry. Of

course some fraction of a field sample limited at R_F=21.2 will have redshifts sufficiently close ($<\pm 0.05$ in z) to A370 for our method to assign them as 'members'. However, we expect this effect to be very small since model predictions based on local field luminosity functions (Ellis 1987) indicated that only 18 per cent of the field galaxies in a R=21.2 limited sample will lie in this region close to z=0.37. At most, four of the galaxies classified as members are likely to be $z\sim 0.37$ field galaxies. Our SED classifications therefore *support* the statistical estimates of the field galaxy density in the vicinity of Abell 370 provided by Couch's photographic photometry.

Having confirmed the level of field galaxy contamination in A370, we now independently assess the high blue fractions previously claimed for this cluster using our CCD classifications. Butcher & Oemler (1984) determined the fraction of objects bluer by more than 0.2 mag in rest-frame $B-V$ than an E/S0 galaxy of the same absolute magnitude. For a sample of 107 galaxies drawn from within a 2.2 arcmin radius and limited at $M_V=-20.0$ (which corresponds to $R\sim 22$ for an early-type galaxy at z=0.37) they found $f_b=0.21\pm 0.05$. Couch (1981), on the other hand, decomposed his observed cluster colour distribution into *spiral* (blue) and *E/S0* (red) components similar to the approach taken by Butcher & Oemler (1978b). He measured a 34 per cent spiral fraction for a sample of 184 galaxies gathered within a 2.6 arcmin radius and limited at R_F=21.8 – equivalent approximately to a blue fraction $f_b\sim 0.19$ (a nearby rich cluster of similar concentration has $f_b\sim 0.03$–0.05).

In comparison to these studies, our CCD sample is smaller being drawn from a 3.75×2.0 arcmin area centred on the cluster and reliably (SED) classified to R_F=21.2, though our method uses four pass-bands with data of much higher S/N. Using the classifications of Table 3 and considering only those objects placed at z=0.37, we find the following distribution:

E/S0	Sab	Sbc	Scd	Sdm
59.5 (76 per cent)	4.5 (6 per cent)	1.5 (2 per cent)	12 (15 per cent)	0.5 (12 per cent).

Our CCD data thus indicate a 76:24 per cent division between E/S0s and Sps (Sab–Sdm) whereas Couch observed a 66:34 per cent division within his larger 2.6 arcmin radius. Some of the difference will be due to the different sizes of the regions sampled and to gauge this we have evaluated the mean local galaxy density in each area since it it this quantity that is the prime determinant of morphological mix (Dressler 1980). We find the local density (as defined by Dressler) to be, on average, a factor of 2 higher in the CCD region than in the more extended region studied by Couch. Accordingly, the fraction of spiral galaxies is expected to be lower with Sp (CCD)=−11 per cent compared with Sp (Couch)=15 per cent. The reduced (24/34=0.70) spiral fraction observed in our CCD sample is in very close agreement with this expected difference (11/15=0.73). In other words, we observe the *same* excess (via percentage observed/percentage expected) as did Couch.

Examining now the nature of the blue members in A370, we first comment on the distribution in type of the ~19 objects in our CCD sample classified as spirals. Rather than being distributed evenly amongst the four spiral classes (Sab, Sbc, Scd, Sdm), we find the galaxies to be predominantly (65 per cent) Scd's. This suggests a further manifestation of the BO-effect since late-type systems are rarely seen in the rich cluster environment at the present epoch. Furthermore, the SEDs of these objects indicate that they are very blue and are therefore obvious candidates for Butcher & Oemler's claimed blue galaxy population. To investigate this more quantitatively, we have determined (by interpolating between our reference E/S0 and the Sp SEDs) the SED representative of Butcher & Oemler's blue galaxy limit (see above). This allows us to identify 'blue' galaxies on the basis of their *overall* spectral energy distribution (rather than just one colour) and at the same time retain consistency with Butcher & Oemler's definition. In effect the method isolates objects with SEDs of type Sbc and later.

Out of a total of 78 cluster galaxies in our CCD sample we find that 13 fall into this *blue* galaxy

category thereby giving a blue fraction of 17 per cent. This value is probably an underestimate in the area studied by Butcher & Oemler for the same reasons that applied to the comparison with Couch's data; we therefore *confirm* Butcher & Oemler's claim of a 21±5 per cent fraction of blue galaxies in A370.

4.2 COLOUR–MAGNITUDE RELATIONS

The motivation behind constructing CM diagrams is threefold:

(i) It provides an extra check on our spectral classifications since we only expect E/S0 galaxies to display the CM effect.

(ii) The scatter of the E/S0 galaxies around the mean relation is a useful indicator of the homogeneity of the E/S0 population.

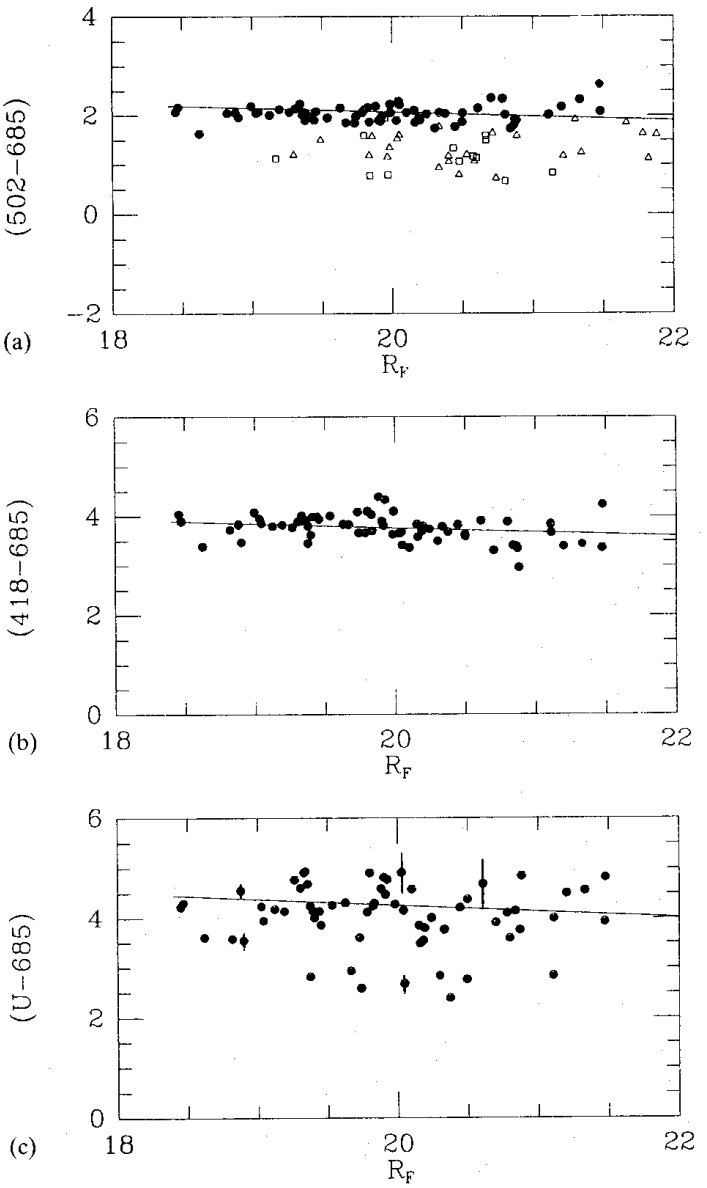

Figure 4. Colour–magnitude diagrams for galaxies classed photometrically as members of Abell 370. Data are shown to R_F=21.7 but the samples are complete only to R_F=21.2. Solid lines show the expected locus of the present-day E/S0 relation adopting the reddening and UV energy distribution discussed in the text. (a) 502–685: all members including E/S0s (filled circles), spirals (triangles) and unclassified possible members (squares). (b) 418–685: E/S0s only. (c) *U*–685: E/S0s with representative error bars derived from Section 2.3.

(iii) It may be possible to make absolute comparisons with the relation seen for nearby cluster E/S0s and hence monitor luminosity and colour evolution with large samples of galaxies drawn from representative portions of the cluster luminosity function.

Fig. 4 shows the CM relation for various colours with the SED classifications from Table 3 indicated by different symbols. Starting with the 502–685 relation (restframe 366–500), note how the E/S0s define a tight sequence close to that predicted on the basis of the method described in

Table 5. Spectroscopic and SED classifications for other clusters.

Cluster	CCD	Spectroscopy z	Source	SED Class	z	Comments
A1942	26	0.145	H	Sab	0.2	
	56	0.145	H	Sab	0.2	
	84	0.225	H	Scd	0.25	
	1	0.224	H	E/S0	0.2	
	33	0.307	CEM	E/S0	0.3	
	16	0.217	CEM	E/S0	0.15	
A1525	1	0.25	CEM	E/S0	0.25	
	2	0.257	CEM	E/S0	0.25	
	3	0.1	CEM	E/S0	0.1	
	46	0.257	CEM	E/S0	0.25	
	61	0.26	CEM	E/S0	0.25	
	16	M star	CEM	–	–	poor SED fit
AC103	1	0.113	SECG	Scd	0.2	
	2	0.311		E/S0	0.3	
	3	0.312		E/S0	0.3	
	4	0.310		E/S0	0.3	
	13	0.310		E-Sab	0.3	
	36	0.309		E/S0	0.25	
	43	Star		–	–	poor SED fit
	49	0.333(EM)		Scd	0.3	
	144	0.303		Sab	0.25-0.3	
	145	0.312		Sab	0.3	
	15	0.31		E/S0	0.3	
	39	0.31		E/S0	0.3	
	20	0.31		E/S0	0.3	
	12	0.31		Sab	0.25-0.3	
	22	0.31		E/S0	0.3	
	17	0.31		E/S0	0.3	
	47	0.31		E/S0	0.3	
0016+16	62	0.30	DG	E/S0	0.3	DG184
	2	0.54		E/S0	0.55	DG149
	1	0.54		E/S0	0.55	DG144
	63	0.54		Scd	0.4-0.6	DG215 [OII] em
	144	0.53		Sab	0.3	DG37 Balmer abn
	38	0.65?		Sab	0.3-0.4	DG207
	7	0.54		E/S0	0.55	DG156+157
	6	0.54		E/S0	0.55	DG170
	11	0.21		Scd	0.1	DG116
	18	M Star		E/S0	0.6	DG114
	59	0.21		Sab	0.2-0.3	DG198
	56	0.39		Sab	0.1-0.2	DG232
	3	0.54		Sab	0.55	DG135
	50	0.55		E/S0	0.55	DG217
	37	0.54		E/S0	0.45-0.6	DG203
	64	0.56		E/S0	0.3	DG224 Balmer abn
	42	0.53		E/S0	0.3-0.4	DG200

HL – Henry & Lavery (private communication).
DG – Dressler & Gunn (private communication).
CS – Couch & Sharples (1987) in press.
SECG – Sharples, Ellis, Couch & Gray (1985).
CEM – Couch, Ellis & MacLaren (unpublished).

Table 6. Spectroscopy of A370.

CCD	BO	R_F	z	Source	Features	SED class
107	9	18.45	0.374	M	E	E/S0
			0.365	BO	sp	
1	10	18.47	0.379	M	E	E/S0
53	15	18.62	0.201	HL	–	z=0.25 E/S0
			0.250	M		
81	–	18.82	0.37	M	E	E/S0+UV
125	21	18.88	0.366	HL	–	E/S0
			0.370	M	E	
20	29	18.90	0.370	HL	–	E/S0+UV
			0.371	M	E+A	
			0.37	CED	E	
47	34	18.99	0.378	M	E	E/S0
42	24	19.03	0.375	M	Sp	E/S0
31	26	19.04	0.382	M	E	E/S0
32	43	19.12	0.383	M	E	E/S0
66	39	19.17	0.374	HL	sp	Scd
			0.375	M	sp	
			0.375	BO	sp	
29	41	19.19	0.375	HL	–	E/S0
			0.377	M	E	
49	45	19.27	0.368	M	E	E/S0
137	56	19.29	0.177:	HL	–	Sab
			0.17	M	sp	
102	49	19.38	0.378	M	sp	E/S0+UV
46	256	19.67	0.37	M	sp (weak)	E/S0+UV
68	66	19.41	0.370	M	sp	E/S0
			0.361	HL	E+A?	
			0.37	CED	E	
27	105	19.73	0.37	M	sp (weak)	E/S0+UV
86	106	19.74	0.371	M	sp (weak)	E/S0+UV
4	58	19.80	0.460	M	E	E/S0
50	99	19.83	0.548	M	E	E/S0
70	128	19.83	0.358	HL	sp	Scd
62	107	19.85	0.37	CED	E	E/S0+UV
108	176	19.96	0.222	HL	–	Scd
124	151	19.97	0.253	HL	–	z=0.2–0.4 Scd/Sdm
93	128	19.98	0.358	HL	sp	Scd
90	165	20.03	0.386	HL	?	Scd
79	149	20.04	0.382	M	sp	E/S0–Sab
69	131	20.05	0.37	M	sp (weak)	E/S0+UV
138	145	20.05	0.376	HL	sp	Sbc
19	164	20.33	0.227	HL		Sbc/Scd
140	201	20.47	0.230	HL		Scd/Sdm
85	239	20.53	0.384	HL	sp	Scd
139	231	20.74	0.31	HL		Scd
57	280	20.93	0.328	HL		E/S0+UV

Sources:
HL – Henry & Lavery (1987) preprint.
M – Mellier, Fort & Soucail (1987) preprint.
BO – Butcher & Oemler (private communication).
CED – Couch, Ellis & D'Odorico (unpublished).

Features:
E – E/S0 with no emission, large 4000 Å break, red spectrum.
E+A – as E/S0 with Balmer absorption lines.
sp – [OII] emission or Balmer absorption lines.

General notes:
(i) Spectral features for HL have been deduced from their published spectra.
(ii) All SED classifications have z=0.35–0.40 unless otherwise indicated.

Section 3.2(b) and including our adopted reddening. Had reddening been ignored, the predicted line would be bluer by 0.15 mag and almost all E/S0s would lie redward of the prediction.

In the colour 418–685 (restframe 305–500), the relation shows more scatter as expected from errors associated with weaker signal. Again the slope and absolute position of the E/S0 sequence is in excellent agreement with the predictions incorporating Couch's reddening. Of course at $z=0.37$ it might be expected that some colour evolution may be detectable in the early type population with our data of high precision. Current models (e.g. Bruzual 1985) suggest that this would change the colours in the opposite sense to galactic reddening, namely, bluer in the past. To allow *any* colour evolution longward of 300 nm over the past 4–5 Gyr one would have to *increase* the galactic reddening, which is already at a value larger than standard estimates.

Finally, in U–685 (restframe 270–500) the E/S0s show a marked increase in scatter over that seen in the other diagrams. As we discussed in Section 2.3, the errors in this colour are strongly dependent on the location of the object in the CM plane. Using our repeat frame analysis we have determined representative error bars for a selection of galaxies in the figure. We see that the E/S0s galaxies are not randomly distributed about the predicted relation [which agrees well with that observed nearby with the *IUE* satellite Section 3.2(b)]. The distribution of galaxies redward of the line is as expected from a consideration of their large errors, but it is important to recognize that the U–685 error blueward of the line is much smaller yet a significant asymmetry in that direction is present.

Taking the photometric errors into consideration, there are ~10 galaxies that lie more than 5σ blueward of the line. We have indicated these as 'E/S0+UV' in Table 3. These galaxies are identified in Plate 1(a) alongside the UV image in Plate 1(b). As in 0016+16, we therefore find a subset of E/S0 galaxies with a significant enhancement of UV flux but which are indistinguishable from the remainder at optical wavelengths. The effect is more statistically significant than in 0016+16.

5 Spectroscopy of galaxies in Abell 370 and other clusters

Since the initiation of this project in 1983, several groups including ourselves have obtained spectra of a limited number of galaxies in the field of Abell 370. The most extensive lists are those of Mellier *et al.* (1987) and Henry & Lavery (1987), with smaller catalogues available from unpublished work of Butcher & Oemler and Couch, Ellis & D'Odorico. Each group used multi-slit techniques.

In parallel with this development, spectroscopy has also become available for a number of galaxies in other clusters for which we have multicolour CCD data. These include the clusters studied in Paper I – namely A1942 ($z=0.22$, Henry & Lavery, private communication), A1525 ($z=0.253$, Couch, Ellis & MacLaren, unpublished) and AC 103 ($z=0.31$, Sharples *et al.* 1985; Couch & Sharples 1987) and that studied in Paper II – 0016+16 ($z=0.54$, Dressler & Gunn, private communication). We are now in a good position to compare the spectroscopic and SED classifications for 86 objects with $18<R<22$ and a wide range of z. The comparison of spectroscopic and photometric classifications for the clusters surveyed in Papers I and II is summarized in Table 5 and the A370 comparison based on the analysis of this paper is listed separately in Table 6.

Although spectroscopic identifications are valuable for a number of studies related to those discussed above, it is important to recognize that these samples are not usually complete in any obvious sense – for example, it is easier to recognize emission lines at low S/N and thus in a magnitude limited sample, successful spectroscopy is often biased towards bluer galaxies at the faint end. An additional limitation on the choice of objects is the need to fill up the available space on the detector with spectra from the multislits. Furthermore, spectroscopic identifications

become extremely difficult to determine reliably beyond $R_F \sim 20$–20.5, about 1.5 mag brighter than our completeness limit and a magnitude brighter than our classification limit.

Here we shall use Tables 5 and 6 to assess the precision of our technique in a number of clusters and then, in A370, to check the conclusions based on our complete and more extensive photometric sample. From the discussion in Section 3.1 we expect an accuracy of ± 0.05 in z and ± 1 in Hubble type for normal galaxies.

Table 5 shows that of 46 objects in four fields, our SED classifications are confirmed to within our stated accuracy in all but two cases. Both discrepant objects are members of 0016+16 attributed by us to a foreground group of galaxies at $z \sim 0.3$. Dressler claims both show strong Balmer absorption lines similar to those seen in the spectra of several galaxies in the cluster 3C 295 (Dressler & Gunn 1983). They have interpreted such objects as galaxies which underwent a burst of star formation ~1 Gyr prior to the time of observation. Such objects can be recognized by the unusual combination of A-type stellar features superimposed on a red evolved stellar population. On the basis of our CCD photometry of 0016+16, it is difficult to see how these two objects could be as red as the archetypal post starburst galaxies in 3C 295. More likely, they represent a class of object intermediate in colour between a normal spiral and a post-starburst galaxy. With more examples, it may become possible to define a mean SED for this class of object and hence incorporate it into our classification scheme.

Before discussing the A370 comparison, where an almost equal amount of spectroscopy is now available, it is important to discuss the target selection methods adopted by the various groups. Henry & Lavery's sample was chosen primarily to attack the Butcher–Oemler question in A370 – they give no detailed discussion on their selection procedure. Most targets are blue, with red E/S0-types presumably selected to complete the detector area. Mellier *et al.* used A370 as a target for their new multi-aperture system on the Canada–France–Hawaii telescope and have similar selection methods. The exception here is the sample of Couch, Ellis & D'Odorico who selected, in a single multislit exposure with the ESO 3.5-m EFOSC system, a number of E/S0s classified via the SED system to have ultraviolet excesses.

Bearing in mind that these samples are generally biased towards the bluer objects, where our technique is less accurate, we begin by assessing the accuracy of the SED classification scheme as far as redshift estimation is concerned. We note that where comparisons can be made between different *spectroscopic* observers (8 galaxies) the agreement is excellent except in one case (CCD 53). However, the SED method fails to achieve its claimed ± 0.05 precision in six cases, and we discuss these below.

(i) CCD 4 and 50 are claimed by Mellier *et al.* to be background E/S0s whereas we place them as E/S0s in the cluster. Given that both are relatively bright ($R \sim 19.8$) with near-perfect fits we find this a surprising discrepancy, particularly when one considers our perfect success rate for E/S0s in 0016+16 *all* of which were fainter.

(ii) CCD 137: Henry & Lavery and Mellier *et al.* find this galaxy to be a foreground object whereas the SED method places it as a spiral member. The 502 flux is too strong by about 0.5 mag for the lower redshift but if this point is ignored there *is* a classification ambiguity using the remaining colours.

(iii) CCD 108: Henry & Lavery claim this galaxy has $z = 0.222$ whereas the SED method places it as a blue member of the cluster. We note that there are five late types in the spectroscopic sample to $R = 20$ (members and non-members) but this is the only discrepancy. Re-examining this and the two similar cases fainter than $R = 20$ (CCD 19, 140), it is clear that the error in redshift from the SED method for late types is a strong function of the UV flux. When the 418–502 colour is blue, the near-UV minimum is removed, the SED becomes linear and a representative error for redshift precision seems to be about ± 0.15.

When comparing SED and spectroscopic type *classifications*, it is important to understand the rather different criteria that are being used. Spectroscopic classifications are grouped into three divisions: E (red spectrum with no indications of recent or on-going star formation), E+A (red spectrum with Balmer lines superimposed) and Sp (blue spectrum with [O II] or other indications of on-going star formation). In the SED method, classifications are assigned purely by colour. Thus a red galaxy encountering a small burst of star formation would be apparently discrepant on the two schemes. It is also important to stress that the E+A classification applies only to *red* spectra with Balmer lines and not to all spectra showing such lines, many of which are normal spirals. In fact, there are only two serious disgreements between the spectroscopic and SED type classifications. Two bright ($R\sim19$–19.4) red members (CCD 42 and 68) are clearly E/S0 in the SED system yet Mellier *et al.* claim to see spiral features. These galaxies show no ultraviolet excess either, though it is interesting to note several other red galaxies claimed to be E+A or to have weak spiral features have an ultraviolet excess (see below).

Thus *if* the spectroscopic identifications are secure, the SED method has a success rate of at least 90 per cent in a sample of ~80 galaxies in the range $R\sim18$–22. Understandably the uncertainties increase as one proceeds to late types. In Table 3, we must consider the possibility that some fraction of the bluest galaxies attributed to the cluster might not be members. On the basis of their relatively small samples, the spectroscopic workers have argued that this effect is small but the identification, by Henry & Lavery, of four late-type galaxies in a foreground clump at $z\sim0.20$–0.25 has prompted us to re-examine the question of contamination.

To $R_F=21.2$, there are 25 galaxies classified by the SED method as late-type spirals (of any redshift) and 11 have spectroscopic redshifts; of these four are non-members. The remaining 14 have been re-analysed using the SED method with the particular question in mind of whether they are at $z=0.23$ or $z=0.37$. However, a careful re-examination of the SEDs indicates that at most three could be at the lower redshift, six are definitely at the higher redshift and for a further four it is impossible to decide – one is at a different redshift. Thus, in total, out of the 25 blue galaxies to $R=21.2$ at least seven spectroscopic and a further six photometric redshifts indicate blue cluster members. Contamination from the $z=0.23$ group is about half this level. The blue fraction determined from the SED method thus could, in the worst case, have a maximum uncertainty of 30 per cent, namely $f_b\sim0.2\pm0.06$. Thus *there are at least three times as many blue galaxies in the cluster as expected for its richness and central concentration*.

Turning to the ultraviolet excess (UVX) E/S0s, of which there are seven that have been studied spectroscopically, it is interesting to note that all but one (CCD 56) are claimed to be spectroscopic members and in five of these cases, weak spiral features are noted. As in 0016, there seems sound evidence linking the ultraviolet flux to a recent enhancement of star formation. We now discuss this possibility in detail.

6 Discussion

The consistent theme in both Paper II and this work is the discovery that some early type galaxies show an enhanced UV flux. In Paper II we were content to show the effect was significant and not an artefact of any instrumental effect. We also briefly explored two possible explanations. Here we examine these more quantitatively.

For 0016+16 we first suggested that the UV excess was akin to a weak Butcher–Oemler effect manifesting itself only in our shortest wavelength band. This seemed appealing because the cluster has a surprising absence of any optically blue members and thus in this way it might be possible to reconcile the Butcher–Oemler effect as a universal phenomenon at different stages of development. Indeed, the proportion of UVX E/S0s in 0016+16 to the total red population to $F<22$ is roughly comparable to the proportion S0s to E+S0s seen in present-day rich clusters.

Furthermore, 0016+16s X-ray flux is unusually high (White *et al.* 1981) and would support the contention that gas stripping in this cluster was at a more advanced stage of development than in the archetypal B–O clusters (e.g. Cl 0024+16 and 3C295). The appearance of a similar phenomenon alongside a substantial blue excess in Abell 370 indicates that such a simplified picture cannot be correct *unless* different galaxies are simultaneously at various stages of the transition from spirals to S0s.

The second suggestion made in Paper II was that there might be an overall enhancement of star formation in the early-type population at $z>0.3$, along the lines indicated by traditional arguments (*cf.* Bruzual 1984; Ellis 1984), but that *not all early-type galaxies share precisely the same star formation history, even within a single cluster*. The kind of processes responsible for the different behaviour seen in each galaxy then requires explanation. In this case the UVX phenomenon would be a different physical process from that required to explain the B–O effect. The substantial differences in blue fractions observed between 0016+16 and other high-z clusters then remains unanswered, though possibly some explanation along the general lines indicated above might be feasible.

Here we examine a further more interesting possibility that the B–O blue excess, the post-starburst (PSB) and UVX phenomena are various stages along a single evolutionary track leading towards a passively evolving red galaxy. Again, in Abell 370, different galaxies would have to be simultaneously different 'snapshots' of the same basic process. The variation is not an overwhelming difficulty to come to terms with since in many respects it would be most surprising if galaxy evolution proceeded methodically with redshift for all early types regardless of luminosity and environment.

In this regard it is interesting to question whether the UVX E/S0s show any hint of environmental effects in their spatial distribution, e.g. as compared with the remainder of the red members. With the small sample currently available in 0016+16, there was no convincing difference. In Abell 370, however, there is a hint of a circular distribution some 300 kpc (assuming Hubble's constant is 50 km s^{-1} Mpc^{-1}) from the cluster centre (see Plate 1a and b). Indeed there is only *one* UVX E/S0 within this ring as compared to ~20 normal E/S0s. However, the same behaviour is not seen in 0016+16, where one of the bright pair of central galaxies is UVX. Certainly there is the possibility that the effect arises in interactions. In Abell 370 there is a distinct congregation of UVX galaxies associated with the arc-like structure (*cf.* Lynds & Petrosian 1986).

We now examine the possibility that the PSB and UVX phenomena may be linked and explore quantitatively what burst strengths and evolutionary time-scales might be needed. Our technique is to extend the standard Bruzual (1980, 1984) models which are able to follow the evolution of various stellar populations as a function of time. Couch & Sharples (1987) have been able to make precise spectral predictions by linking the intermediate dispersion stellar library of Jacoby, Hunter & Christian (1984) to these models. We are therefore able to examine, simultaneously, the UV excess at ~250 nm (using the models in their original form) *and* the spectral appearance in the optical region. One of the more bewildering aspects of the UVX phenomenon is the near absence of any change in the optical photometry, e.g. the 400 nm break. We also use this technique to monitor at what stage in the lifetime of a typical burst can the UV excess seen in Abell 370 and 0016+16 be compatible with a spectrum at ~400 nm typical of luminous galaxies in nearby clusters, or the appearance of the Hδ line in the case of the PSB galaxies.

Fig. 5 shows the evolution of two bursts of 5 and 10 per cent (in terms of fractional mass consumption) superimposed upon an old stellar population. In terms of Bruzual's parameters, we added a constant 1 Gyr burst at age 9 Gyr to a c-model with a 1 Gyr initial burst at the formation redshift (the model assumes $H_0=50$, $q_0=0.01$). At each stage in the model we calculate the rest-frame UV excess as follows. We de-redshift the U+RCA CCD response function by $1/(1+z)$ and

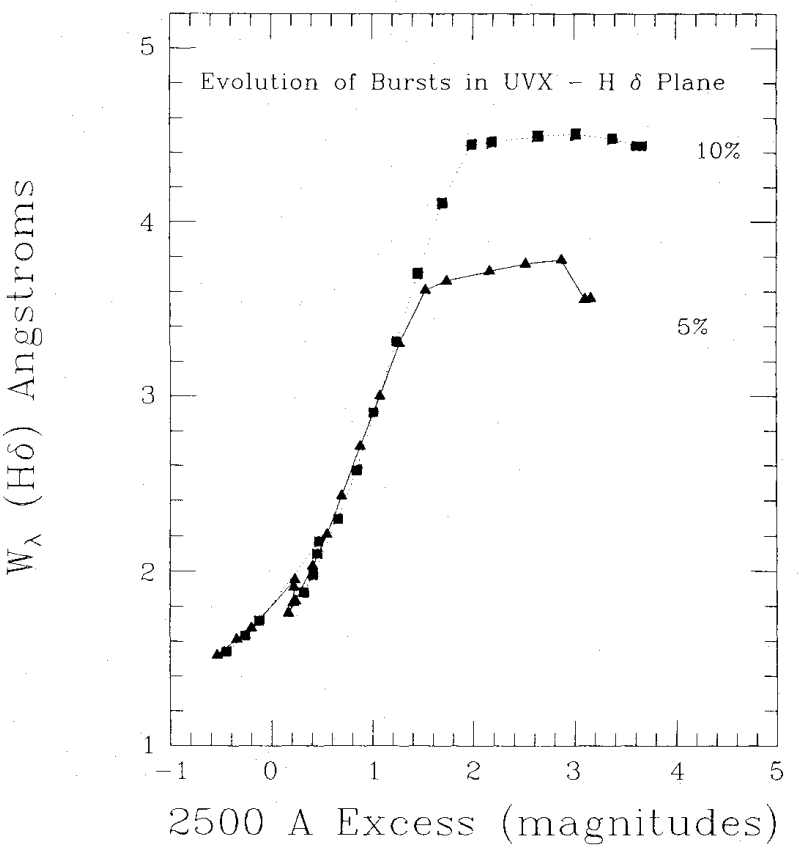

Figure 5. Evolution of the UV excess and Hδ equivalent width for a 1 Gyr burst of 5 or 10 per cent strength by mass superimposed on a 9 Gyr old population. The time intervals correspond to time intervals of 0, 0.004, 0.02, 0.08, 0.2, 0.4, 0.6, 0.8, 1, 1.2, 1.4, 1.6, 1.8, 2, 2.2, 2.6, 3, 4, 5 and 6 Gyr after completion of the burst.

integrate the flux through this 250 nm 'filter' in the evolving model. We repeat the procedure for the case where there is no burst at 9 Gyr and refer to the difference as the 'UV excess'. This is preferable to any empirical difference using observed reconciling present-day UV energy distributions of elliptical galaxies with standard Bruzual models.

The Hδ equivalent width is measured from the synthesized spectrum. The technique developed by Couch & Sharples also calculates the number of photons below the Lyman limit for the purposes of emission line predictions. However, that is not important in this case, since within 10^7 yr of the end of the burst, calculations show the emission line contribution to Hδ can be safely ignored.

Fig. 5 shows that the Hδ strength is indeed a good indicator of the strength of the burst for ~0.4 Gyr after the burst ends, but soon after the line decays in a manner irrespective of the burst strength because the final generation of A stars responsible for the Balmer series have evolved off the main sequence. However, the decline in the UV flux is less marked in this subsequent phase from 0.4 to 2 Gyr after the burst ends and offers a valuable way to identify and provide further statistics on the burst phenomenon. For example, our UVX criterion is approximately equal to $\geqslant$0.5 mag on Fig. 5 and thus we predict a clear correlation between the UV strength and the Hδ equivalent width.

If the UVX phenomenon represents a later stage of evolution after a burst of star formation than the PSB red galaxy, then one would expect the optical colours to be at least as red; this is how the UVX galaxies are empirically defined. The models have some difficulty in reproducing the UV excess as well as the red optical colours. For models where the UV excess is ~0.5 mag from

1 Gyr bursts of 5–10 per cent by mass, there is still a small excess of light ~0.1 mag) in 502–685 and a corresponding linear increase in this as the UV excess increases. The correlation between UVX and '502–685 excess' (*cf.* Fig. 4) is very weak. A similar difficulty was encountered by Couch & Sharples in matching the broad-band colours of their 'strong Hδ' galaxies and they discussed the possibility of dust associated with the starburst itself. The other alternative is that the mass function associated with the burst is deficient in intermediate mass stars contributing to the optical colours. Neither are particularly attractive but it requires yet more precise photometry of the UVX galaxies to determine exactly how serious this problem is.

We can only surmise whether the end stage of this evolution is an S0 galaxy or an elliptical. In Paper II we noted that the proportion of UVX objects to the total red population in the cluster 0016+16 was close to that expected for S0s:(E+S0s) from the morphology–density relation. In the case of Abell 370, the UVX:red ratio is lower than this prediction, but this is not surprising when we consider that the cluster also has a large blue fraction. In the scenario envisaged, many of the evolving galaxies in Abell 370 are observed at an earlier, bluer stage than the galaxies in 0016+16. The crucial test will be to obtain high resolution spatial images of each type of galaxy on this evolutionary sequence.

Thompson (1987) has studied two galaxies in Abell 370 from Mauna Kea at resolutions of 0.6–0.9 arcsec FWHM. In his discussion he claims both are representative of 'post-starburst' galaxies

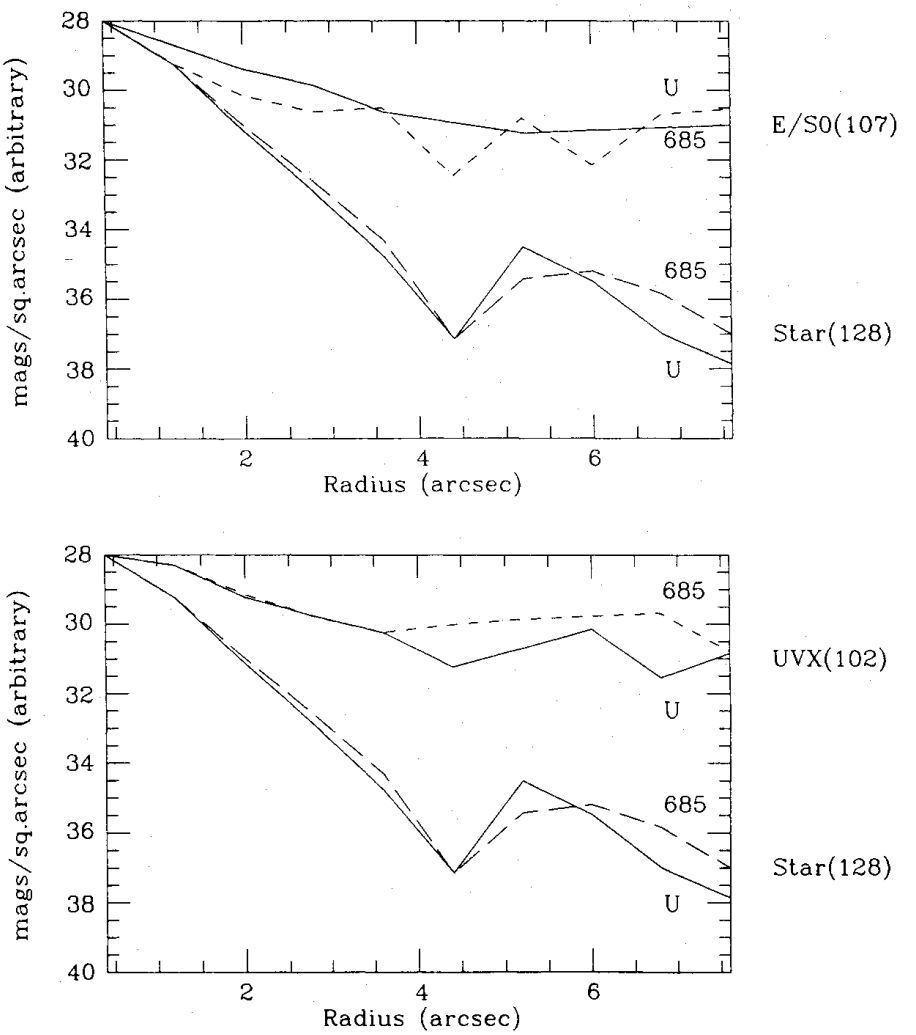

Figure 6. Surface brightness profiles (in arbitrary units) with radius for the brightest representative UVX and non-UVX galaxies in Abell 370.

(Henry & Lavery's spectra of these objects show strong Balmer absorption lines and weak or absent [O II] emission). In our classification system they are markedly different objects. The first (CCD 70=BO 128) is blue at all wavelengths observed by us. We classify it as a member Scd and, if it is part of the sequence described above, it must be in a very early phase soon after the burst has subsided. On the other hand, the second galaxy (CCD46=BO 256) is a UVX E/S0 and intrinsically red in the optical. Both galaxies are claimed by Thompson to have faint apparent companions. Since we believe the UVX phenomenon is a relic of an event that happened at least 2–3 Gyr earlier, the appearance of the companion to CCD 46 is probably of little significance given the short cluster crossing time. However, the *morphological* appearance of galaxies like CCD 46 is a crucial issue – and one Thompson is not yet able to resolve. It would be interesting to image a larger sample of PSB galaxies, particularly the more intriguing PSB galaxies that are intrinsically *red* and, of course, the UVX E/S0s. Unlike the bluer CCD 70, these galaxies have no obvious present day counterpart. In the UVX objects, if high-resolution images reveal the UV excess to be uniformly distributed across each galaxy image, the effect would have to be general to the entire stellar population and thus might indicate elliptical galaxies were undergoing sporadic bursts of 1 Gyr or so in their final decay to passive systems (see Paper II). On the other hand, if there were a UV–optical colour gradient, this might be interpreted via disc light in final decay to a present-day S0.

In fact some of the 0016+16 frames of Paper II were taken in unusually good conditions for the AAT (1.03 arcsec FWHM), comparable in seeing to some of those taken from Mauna Kea. However, the spatial resolution required at the high redshift of 0016+16 remained inadequate by a factor of at least 2 to adequately address the morphological question. In Abell 370, there is some hope at least for the brighter galaxies (1 arcsec at $z=0.37$ corresponds to $\sim$3 kpc) though the observing conditions were not quite so superlative. We have examined image profiles for the brighter UVX and non-UVX E/S0s in both the 685 and *U*-bands with reference to profiles of non-saturated stars (Fig. 6). The profiles were determined from APEX-based software and reduced to differential independent measures within successive annuli assuming radial symmetry. In both 685 and *U*-bands we find no discernible difference between the two samples. However, the interesting frames produced by Thompson (1987) for Abell 370 suggest that with superlative conditions and a simple wavefront tilt-correcting device such a question might soon be answered.

Acknowledgments

We thank Y. Mellier and colleagues, Pat Henry and Russell Lavery, Gus Oemler, David Burstein and Alan Dressler for supplying data prior to publication. We also acknowledge useful discussions with John Lucey, Ray Sharples, Laird Thompson, Jim Rose and Gus Oemler. IM was supported by the SERC during the period of this investigation. WJC acknowledges the award of an Australian National Research Fellowship for part of this work.

References

Bautz, M., Loh, E. D. & Wilkinson, D. T., 1982. *Astrophys. J.*, **255,** 57.
Butcher, H. & Oemler, A., 1978a. *Astrophys. J.*, **219,** 18.
Butcher, H. & Oemler, A., 1987b. *Astrophys. J.*, **226,** 559.
Butcher, H,. & Oemler, A., 1984. *Astrophys. J.*, **285,** 426.
Bruzual, G., 1980. *PhD thesis,* University of California, Berkeley.
Bruzual, G., 1984. *Spectrum Evolution of Galaxies,* p. 67, RAL 84-008, RAL Publications.
Coleman, G. D., Wu, C. C. & Weedman, D. W., 1980. *Astrophys. J. Suppl.*, **43,** 393.
Couch, W. J., 1981. *PhD thesis,* Australian National University.
Couch, W. J. & Newell, E. B., 1984. *Astrophys. J. Suppl.*, **56,** 143 (CN).
Couch, W. J. & Sharples, R. M., 1987. *Mon. Not. R. astr. Soc.*, in press.

Couch, W. J., Ellis, R. S., Godwin, J. & Carter, D., 1983. *Mon. Not. R. astr. Soc.*, **205,** 1287.
Dressler, A., 1980. *Astrophys. J.*, **236,** 351.
Dressler, A. & Gunn, J. ER., 1982. *Astrophys. J.*, **263,** 535.
Dressler, A. & Gunn, J. E., 1983. *Astrophys. J.*, **270,** 7.
Dressler, A., Gunn, J. E. & Schneider, D. P., 1985. *Astrophys. J.*, **297,** 70.
Ellis, R. S., 1984. *Spectral Evolution of Galaxies,* p. 122, RAL 84-008, RAL Publications.
Ellis, R. S., 1987. *Observational Cosmology, IAU Symp. No. 124,* eds Burbidge, G. R. & Hewitt, A., Reidel, Dordrecht, Holland, in press.
Ellis, R. S., Couch, W. J., MacLaren, I. & Koo, D. C., 1985. *Mon. Not. R. astr. Soc.*, **217,** 239.
Henry, J. P. & Lavery, R. J., 1987. Preprint.
Jacoby, G. H., Hunter, D. A. & Christian, C. A., 1984. *Astrophys. J. Suppl.*, **56,** 278.
Kron, R. G., 1978. *PhD thesis,* University of California, Berkeley.
Lilly, S. J. & Longair, M. S., 1984. *Mon. Not. R. astr. Soc.*, **211,** 833.
Loh, E. D. & Spillar, E. J., 1986. *Astrophys. J.*, **303,** 154.
Lynds, C. R. & Petrosian, V., 1986. *Bull. Am. astr. Soc.*, **18,** 1014.
Matthieu, R. D. & Spinrad, H., 1981. *Astrophys. J.*, **251,** 485.
Mellier, Y., Soucail, G., Fort, B. & Mathez, G., 1987. Preprint.
Newell, E. B., 1979. *Image Processing in Astronomy,* eds Sedmak, G., Capaccioli, M. & Allen, R. J., Observatorio Astronomica di Trieste.
Newell, E. B., 1982. *Occ. Rep. R. Obs. Edin. No. 10,* eds Stobie, R. S. & McInnes, B.
Oke, J. B., 1974. *Astrophys. J. Suppl.*, **27,** 21.
Pence, W. D., 1979. *Astrophys. J.*, **203,** 39.
Seaton, M. J., 1981. *Mon. Not. R. astr. Soc.*, **187,** 75P.
Sharples, R. M., Ellis, R. S., Couch, W. J. & Gray, P. M., 1985. *Mon. Not. R. astr. Soc.*, **212,** 687.
Thompson, L. A., 1987. Preprint.
Visvanathan, N. & Sandage, A., 1977. *Astrophys. J.*, **216,** 214.
White, S. D. M., Silk, J. & Henry, J. P., 1981. *Astrophys. J.*, **251,** L65.